

ARTICLE OPEN



Record-shattering 2023 Spring heatwave in western Mediterranean amplified by long-term drought

Marc Lemus-Canovas^{1,2}✉, Damián Insua-Costa³, Ricardo M. Trigo^{4,5} and Diego G. Miralles³

The western Mediterranean region experienced an exceptional and unprecedented early heatwave in April 2023. By shattering historical temperature records, especially in the Iberian Peninsula and northwestern Africa, this extreme offers a stark illustration of a drought–heatwave compound event. Here, we investigate the soil moisture–temperature interactions that underpinned this event, using the most up-to-date observations and a robust statistical analysis. Our results reveal that soil moisture deficit preconditions, concurring with a strong subtropical ridge as a synoptic driver, had a key contribution to the amplification and duration of this record-breaking heatwave. Specifically, we estimate that the most extreme temperature records would have been 4.53 times less likely and 2.19°C lower had the soils been wet. These findings indicate that soil moisture content may be a crucial variable for seasonal forecasting of early HW in this region and in other Mediterranean climate regimes that are already suffering an increment in the frequency of compound drought–heatwave events.

npj Climate and Atmospheric Science (2024)7:25; <https://doi.org/10.1038/s41612-024-00569-6>

INTRODUCTION

As record-shattering heat episodes become more frequent worldwide^{1,2}, understanding the regional drivers of specific events becomes vital to enhance preparedness and adaptation. In late April 2023, an extraordinary spring heatwave (HW) hit the western Mediterranean region. In Portugal and mainland Spain, temperatures reached 36.9°C (Mora) and 38.8°C (Córdoba), respectively, breaking the historical records for the month of April³. Similar extremes were also experienced in Morocco and Algeria, where temperatures exceeded 40°C in several locations⁴. The event was characterised by a subtropical ridge and concurred with a prevailing and severe multi-year drought⁵. For instance, in April 2023, Spanish reservoirs were 50% below average⁶ and dam storage in Morocco was at 33%⁷. Concurrently, Tunisia's largest water reservoir (Sidi Salem) was only at 16% of its maximum capacity⁸. Such scarcity of water strongly impacted the agricultural sector, with the Spanish government allocating direct state aid amounting to more than €636 M to support farmers and stockbreeders in the face of the drought⁹. The hypothesis underlying this study is that these antecedent severe dry conditions acted as amplifiers and catalysts for the temperature records, via the reduction of evaporation in favour of surface sensible heat flux¹⁰. Potentially, we could have witnessed a cascading compound hazard¹¹, where pre-existing drought conditions intensified the subsequent heatwave^{12,13}.

The drought influence on heatwave escalation has been previously documented^{14–16}, especially for specific cases, such as the 2003, 2018 and 2019 European^{10,17,18}, and the 2010 Russian¹⁹ summer HWs. For such summer events in temperate regions²⁰ soil moisture during droughts can be highly anomalous compared to the climatological expectation²¹. On the other hand, due to the climatologically dry soil conditions during summer, Mediterranean regimes tend to be less affected by large negative anomalies in soil moisture, and summer heat waves are rather triggered by heat advection from arid regions²². It remains unknown, however, the

degree to which land–atmospheric feedbacks can play a role during the spring season when climatological soil moisture is higher, and thus droughts can be associated with large negative anomalies in soil moisture and sensible heat flux. For this reason, here we delve into the intricate land–atmosphere interactions that characterised the April 2023 event and quantify the role of concurrent soil drought in the extreme temperatures that were recorded across the western Mediterranean region. As such, the objectives of this work are: (1) to identify the surface and synoptic characteristics of this unprecedented spring heatwave; (2) to quantify the influence of soil drought on the energy balance partitioning and air temperature; and (3) to infer the likelihood of occurrence of such event under dry and wet soil moisture preconditions.

RESULTS

Observed characteristics of the April 2023 heatwave

We first examine the conditions during the HW event, including circulation, temperature and soil drought. The concurrence of high geopotential height at 500 hPa (Z500) and 850-hPa temperature (Fig. 1a), together with extremely low soil moisture levels (Fig. 1b), culminated in 4 days (25–28 April) of consecutive records in daily maximum temperature (Tx) in the city of Córdoba (Spain), which reached its absolute maximum on April 27 with a Tx of 38.8°C (Fig. 1c). This is 4.8°C above the previous record registered in 1960. The extremeness of the dry–hot conditions is portrayed by the fact that temperatures at 850 hPa were above the 99th percentile (Supplementary Fig. 1) while soil moisture was below the 1st percentile over extensive areas (white dots in Fig. 1b).

The synoptic situation described in Fig. 1a, dominated by a high-pressure system or subtropical ridge, is a common trigger of heat waves in the Iberian Peninsula²³. However, what denotes the exceptionality of the event is the occurrence of this atmospheric configuration within a background context of extreme drought.

¹CRETUS, Non-linear Physics Group, Universidade de Santiago de Compostela, Galicia, Spain. ²Andorra Research + Innovation, Rocafort 21-23, AD600 Sant Julià De Lòria, Andorra.

³Hydro-Climate Extremes Lab (H-CEL), Ghent University, Ghent, Belgium. ⁴Instituto Dom Luiz (IDL), Faculdade de Ciências, Universidade de Lisboa, 1749-016 Lisboa, Portugal.

⁵Departamento de Meteorologia, Universidade Federal do Rio de Janeiro, Rio de Janeiro 21941-919, Brazil. ✉email: marc.lemus@usc.edu

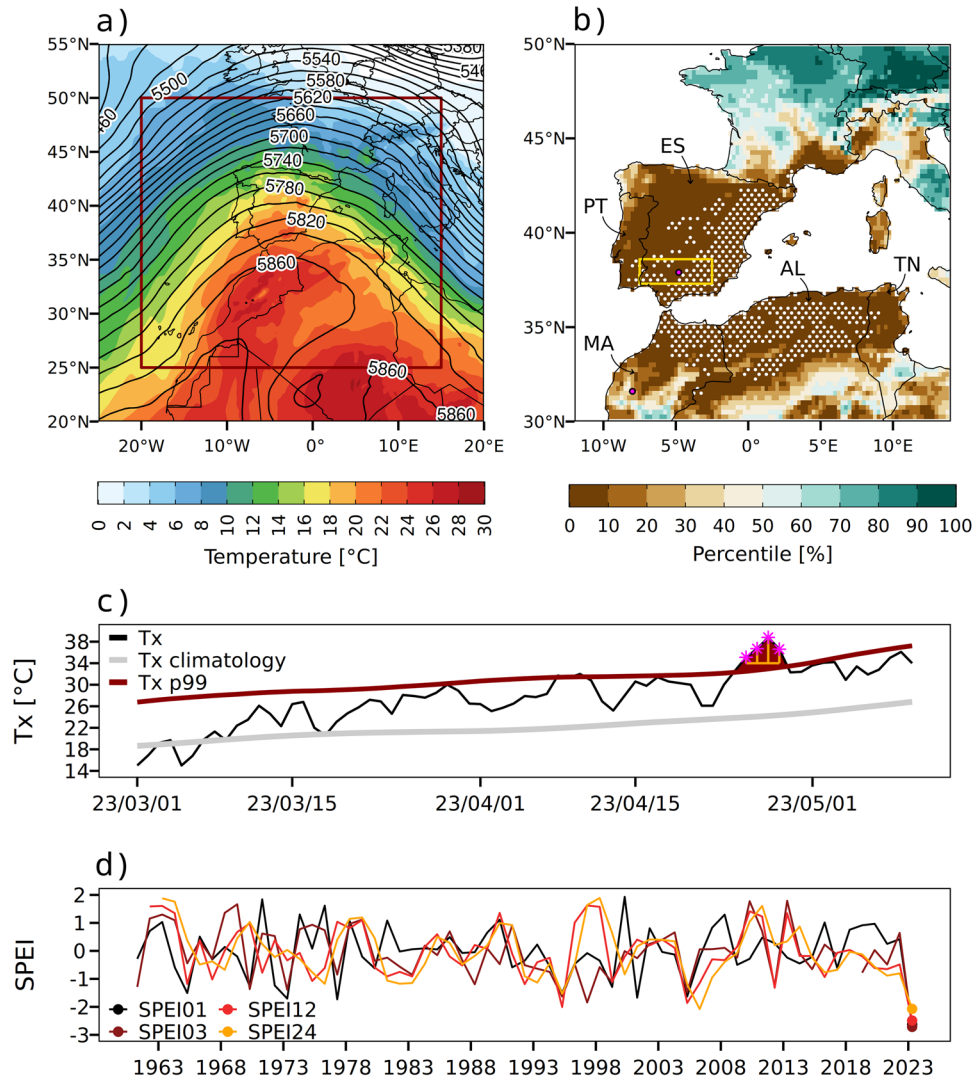


Fig. 1 Climatological context of the April 2023 HW record-shattering in the western Mediterranean region. **a** 850-hPa temperature ($^{\circ}\text{C}$, shading) and 500 hPa geopotential height (dm, contours) at 12UTC on 27 April 2023. **b** Percentile of daily soil moisture at 0–7 cm depth (originally, volumetric fraction) for the 27th of April 2023. White stippling shows areas with volumetric soil moisture lower than the 1st percentile. Percentiles were computed using the 1950–2022 reference period for March, April and May. The yellow box shows the area used to compute the regional time series of both the coupling metric and the soil moisture (see Data and Methods section), while the magenta point inside the box refers to the location of Córdoba (Spain), and the one outside, that of Marrakech (Morocco), both hotspots of the event. The most affected countries are identified with the ISO 3166-1 alpha-2 country codes. **c** Córdoba in-situ time series for daily 2 m maximum temperatures (T_x) from 1 March to 5 May (black line) along with the 1950–2022 T_x 5-day centred running mean (grey) and T_x 15-day centred running mean of the 99th percentile (dark red). Magenta stars denote the 4 consecutive records (25–28 April) and yellow segments show the difference between these new records and the previous ones for April. **d** Regional (averaged over the yellow box in Fig. 1b) Standardised Precipitation and Evaporation Index (SPEI) for 1960–2023 time series for the 4th week of April based on 1-, 3-, 12- and 24-month time scales (dark red and yellow lines, respectively). Data source: ERA5 (**a**), ERA5-Land (**b**), AEMET (**c**), CSIC (**d**).

The latter is clearly depicted by the 1-, 3-, 12- and 24-month Standardised Precipitation Evaporation Index (SPEI) values in the south of the Iberian Peninsula during the last week of April (Fig. 1d), showing that both the short-term and long-term drought affecting this area was unprecedented since 1960.

Soil-moisture temperature coupling during the April 2023 heatwave

We separated the event into three main phases affecting the Iberian Peninsula: (1) build-up (April 22–24), (2) peak (April 26–28), and (3) progressive weakening (April 29–30). The daily π coupling metric²⁴ (see Data and methods section) was used to reveal the influence of soil moisture feedback on temperature (Fig. 2a–c), by decomposing the coupling signal into its surface energy term (H

– H_p), devised to depict the influence of soil drought on the energy balance partitioning, and its air temperature term (T') (Fig. 2a–f). During the first phase (Fig. 2a, d, g), neutral values of the energy term concurred with slightly positive temperature anomalies in the southern end of the Iberian Peninsula, implying low coupling (i.e., low π ; Fig. 2a). The northern coast of Morocco, Algeria and Tunisia also experienced low coupling during this phase. There, dry soil conditions and high incoming radiation led to an increase in surface sensible heat flux, yet cold air advection accompanied by some precipitation (Supplementary Fig. 2) inhibited higher temperature anomalies. On the other hand, during the HW peak (Fig. 2b, e, g), large positive anomalies in both the energy and temperature terms were observed in the southern half of Iberian Peninsula and across large parts of Morocco and northern Algeria (Fig. 2e), indicating strong coupling (high π ; Fig.

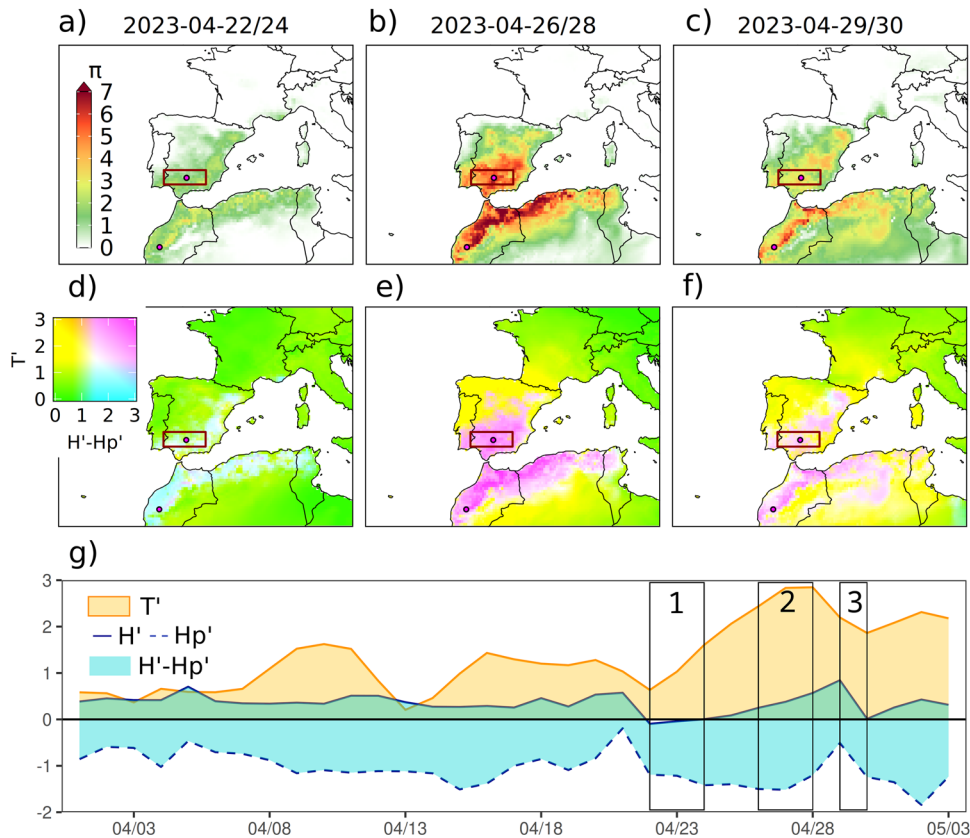


Fig. 2 Soil moisture–temperature coupling during the three identified phases of the April 2023 heatwave. **a** Soil moisture–temperature coupling metric (π) during the three HW phases: build-up (**a**), peak (**b**), and demise (**c**). **d–f** Idem as **a–c** but for the spatial mean values of the temperature (T') and energy ($H'-Hp'$) coupling terms. **g** Time series of both coupling terms from 1 April 2023 to 3 May 2023. The red box in **a–c** and **d–f**, respectively, was used to compute the regional coupling T' and $H'-Hp'$ in southern Iberia, showed in **g**. Black vertical boxes in **g** separate the three HW phases.

2b). Therefore, during the peak of the event, temperature anomalies were strongly affected by higher-than-usual surface sensible heat flux, which was caused by the soil dryness and a surplus of incoming radiation at the surface (i.e., elevated values of $H'-Hp'$) (Fig. 2g). Finally, in the demise phase (Fig. 2c, f, g) a high coupling rate remained in the eastern Iberian Peninsula and in some large areas of North Africa (Fig. 2c). In contrast, in the southern part of the Iberian Peninsula, the degree of coupling decreased drastically during this phase, despite air temperatures still being positively anomalous. This is consistent with the occurrence of light precipitation, and the subsequent lower influence of soil moisture on the extreme temperatures. Above all, the strong concordance found between the two coupling terms during the peak of the event suggests that dry conditions were a critical ingredient in defining this episode as a historically unprecedented HW. Note that the level of soil moisture–temperature coupling (π) obtained for the 2023 April event had not been previously recorded in southern Iberia (Supplementary Fig. 3). Likewise, the same applies to the energy term ($H'-Hp'$), as shown in the inset of Supplementary Fig. 3.

Storylines of the heatwave under different soil moisture preconditions

In our endeavour to determine the influence of soil desiccation on the intensification of the event, we employed the flow analogues technique (see Data and Methods.). For clarity, flow analogues refer to days from a historical period, where atmospheric patterns are closely related to those of a specific event—in this instance, the HW peak spanning 26–28 April. These analogues enable us to establish how similar atmospheric conditions in the past, under

two differentiated soil moisture states (wet and dry), influenced surface temperature dynamics. Thus, to confirm and further quantify the role played by soil desiccation in the amplification of the event we selected flow analogues based on the 1950–2022 period, for each day of the HW peak and reconstructed the associated T_x anomalies (Fig. 3). We disentangled the influence of soil drying by distinguishing between analogue days preceded by dry and wet conditions based on soil moisture anomalies averaged over the previous 15 days and across the south of the Iberian Peninsula (box in Fig. 3a–c)—see Data and methods section.

Results indicate that flow patterns analogous to those observed during the April HW peak tend to result in warmer conditions when preceded by dry conditions (Fig. 3a, b). In other words, conditioned on the experienced atmospheric circulation, soil moisture deficits promote further warming (Fig. 3c, d). It is important to stress that prior to the analysis we removed the linear trend from the soil moisture time series. In addition, the areas of greater amplification due to soil desiccation preconditions coincide with the areas of greater soil moisture–temperature coupling during the peak of the event (Fig. 2e). Specifically, the difference between both groups of analogues exceeds 1°C in most of the Iberian Peninsula (Fig. 3c), being of the order of 2°C on average in the south (Fig. 3d), and locally, close to Córdoba, even exceeding 3°C (Fig. 3c). Regarding the different circulation behaviour under dry and wet precedent conditions (Fig. 3e), the April 2023 HW peak it is slightly closer to a dry-like preconditioned circulation than a wet-like one, although no relevant differences are shown.

Finally, the temperature difference shown in Fig. 3 between dry and wet analogues is not to be interpreted as a measure of the

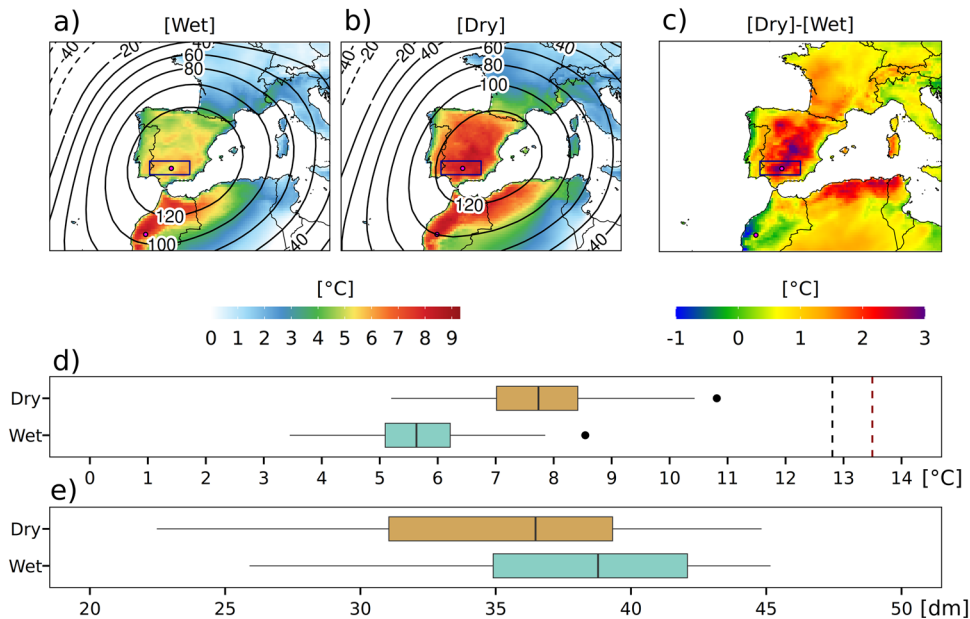


Fig. 3 Wet and dry circulation analogues of the April 2023 heatwave (HW) peak. Mean Z500 (m, contours) and Tx (°C, shading), presented as anomalies with respect to 1950–2022, reconstructed for the HW peak (26–28 April 2023) from daily flow analogues of Z500 over the western Mediterranean domain (solid box in Fig. 1a). We separate analogues preceded by **a** wet (above the 66th percentile) and **b** dry (below the 33rd percentile) average soil moisture conditions at 0–7 cm in the southern Iberian Peninsula (black box in **a–c**) during the previous 15 days. **c** Difference between **b** and **a**. **d** Flow-conditioned distributions of the mean Tx anomalies for the April HW peak over south Iberia preceded by wet and dry conditions (y-axis). Vertical black (red) dashed lines depict the regional mean (maximum) values observed during the event peak. Boxes show the interquartile range and whiskers span the 1st–99th percentiles, with points denoting the analogue maximum Tx. **e** Flow-conditioned distributions as **d** but for geopotential height anomalies at 500 hPa over the domain used to search analogues shown in Fig. 1a (20W–15E, 25N–50N).

warming effect of soil drought during the specific April 2023 HW event, but rather as a representative difference between wet and dry soils in April 2023-like atmospheric configurations. Therefore, we implemented an additional analysis to quantify the role of land–atmosphere interactions for this episode. To this end, we first estimated the changing likelihood of the maximum regional Tx reached during the HW peak (Fig. 3d, red vertical dashed line), by fitting the maximum value of each HW peak reconstruction repeated 5000 times to a Generalised Extreme Value (GEV) distribution (See Data and Methods). That is to say, we calculate the probability of reaching the maximum observed Tx anomaly value (13.5 °C) for both the dry and wet analogue groups and evaluate the difference. The process was repeated for different time windows in which to search for analogues to test the robustness of the method. Our results show that the event was 4.53 times (standard deviation: 0.87) more likely due to the drought context prior to the event (Fig. 4a). In addition, using this approach we were able to estimate that the maximum Tx reached for this event under dry preconditions was 2.19 °C (standard deviation: 0.17 °C) higher than if conditions had been wet (Fig. 4a). In short, our results demonstrate that soil moisture deficits in the Iberian Peninsula intensified the warming expected from the anomalous circulation observed during the peak of the April 2023 HW.

DISCUSSION

Our findings demonstrate that the severe drought conditions preceding the April 2023 HW were a crucial factor in explaining the exceptional temperature records. We clearly identified the synoptic driver of the situation as a pronounced subtropical ridge pushing warm air northwards into the Western Mediterranean. However, even though the subtropical ridge affected a wide area, the most extreme temperatures were recorded in the south of the Iberian Peninsula, as well as in large parts of northern Morocco

and Algeria, which were both the areas with the largest negative soil moisture anomaly and the highest soil moisture–temperature coupling, suggesting a significant contribution of soil desiccation to the extreme temperature reached in this event. We have also shown that the probability of reaching such an extreme regional maximum Tx in the southern Iberian Peninsula would have been 4.53 times lower had the soils been wet. Nevertheless, we must acknowledge that the top value of the regional maximum Tx, obtained with the analogue dry subset, falls roughly 2.5 °C colder than the observed value for the peak HW phase (upper black dot vs vertical red dashed line in Fig. 3d). Thus, it is likely that other mechanisms might have also contributed to exacerbating the 26–28 April HW amplitude. In this regard, it is worth mentioning the development of marine heatwave conditions in the eastern Atlantic and eastern Mediterranean clearly visible through the high SST anomalous values in these sectors (Supplementary Fig. 4). Further research, using regional circulation models, is required to better access the role SST's may play in future record-shattering heat events.

Climate projections indicate a significant worsening of drought and aridity conditions in the southern Iberian Peninsula^{25,26}, thus compound dry–hot events are expected to aggravate²⁷, leading to alarming consequences such as the increase in fire risk in the area²⁸. This area is therefore a hotspot in the context of climate change, where further research on HW amplification mechanisms is needed to guide decision-makers in implementing mitigation and adaptation measures through, for example, land use management²⁹.

The methodology employed in this study could help to this end. The application of the analogues technique to the study of land–atmosphere feedback remains novel¹⁸, and here we propose its combination with a statistical technique that follows the same logic as the climate change attribution risk approaches^{30,31}. This allows us to quantify the drought-induced temperature amplification in specific cases in a much less computationally expensive

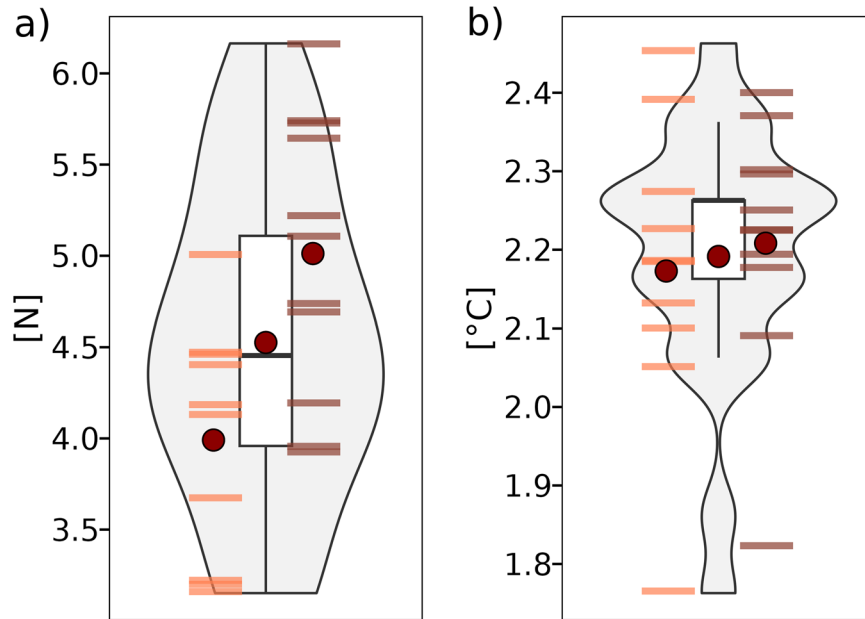


Fig. 4 Estimated increase in temperature and likelihood of maximum Tx under dry and wet preconditions. **a** maximum Tx and **b** probability under dry SM compared to wet SM preconditions, estimated by means of a GEV fit. Horizontal orange lines represent the GEV prediction for the sequence of 21- to 30-day time windows centred in the peak of the event, whereas brown lines show the same but for the 31- to 40-day time windows, respectively. There is one horizontal line for all days comprising the sequence from 21 to 40 (see Analogues experiment in Data and Methods section for further details). Dark red points indicate the mean value of the entire distribution (middle), whereas left and right points refer to the two-time windows above mentioned. Boxes show the interquartile ranges and whiskers span the 1st–99th percentiles.

and more observational way than other methodologies, such as atmospheric or climate model simulations, which are also more subject to model errors^{32,33}.

Importantly, our findings indicate that in terms of land–atmosphere coupling during extreme events, semiarid regions in spring can behave like temperate regions during summer. It is well known that summer soil moisture anomalies can play an important role in the intensity of HWs at higher latitudes (e.g., 2003 France, 2010 Russia^{15,19}, central and northern Europe^{17,18}), but in drier regions like southern Spain, the room for soil dryness to induce temperature anomalies is limited, since dry soils are the norm during summer. However, our results show that in spring, when soil moisture content is more variable, HWs can indeed be significantly enhanced by antecedent drought conditions. Therefore, our findings suggest that in these semiarid regions, including other Mediterranean climate regions where hot–dry compound events are aggravating (e.g., California, central Chile), soil moisture may be a good diagnostic of spring HW risk and hold potential for subseasonal HW forecasting.

METHODS

Observational data

Córdoba daily maximum temperature (Tx) time series was retrieved from the Spanish meteorological service (AEMET), specifically from AEMET Open Data (<https://opendata.aemet.es/>). To access these data through the AEMET API we used the *climaemet* R package³⁴.

Standardised Precipitation Evaporation Index

To characterise the unprecedented drought conditions over southern Iberia (Fig. 1d), we use 1-, 3-, 12- and 24- SPEI³⁵ time scales calculated for the 4th week of April and extracted directly from the SPEI Spain Drought monitor, freely available at <https://monitordesequia.csic.es> at 1 km spatial resolution from 1960 to

the present. The SPEI Spain Drought Monitor provides near real-time SPEI estimates at different temporal scales, computed at the end of each week for the Spain mainland. AEMET and SIAR weather station networks were used to feed the drought monitor.

ERA-5 Land

Daily Tx and volumetric soil moisture (in $\text{m}^3 \text{m}^{-3}$) in a layer of 0 to 7 cm depth were extracted from the European Centre of Medium-range Weather Forecast (ECMWF) ERA-5 Land reanalysis³⁶. SM was used to characterise the soil moisture conditions prior to the event and to disaggregate dry and wet episodes in the flow analogues experiment, while Tx was used as a predictor in this experiment. Note that to compute the coupling metric in Fig. 2, daily mean temperature (Tm) was used instead of Tx. Moreover, evaporation, potential evaporation and both surface net solar and thermal radiation were also used to this end. Anomalies were computed with respect to the climatological seasonal cycle in the reference period 1950–2022. All these data were presented at a horizontal resolution of $0.25 \times 0.25^\circ$.

ERA-5

Meteorological fields for atmospheric levels were retrieved from the ERA-5 reanalysis hourly dataset³⁷, starting in 1950. We averaged the original data to a daily format. Air temperature at 850 hPa (T850) and geopotential height at 500 hPa (Z500) were resampled to a $1 \times 1^\circ$ horizontal resolution grid, due to no finer resolution was needed. These fields were used to: (i) characterise the synoptic drivers of the HW, and (ii) for Z500 only, to perform the analogues experiment. Specific methods for products derived from these variables are explained below. Percentiles for Supplementary Fig. 1 were computed with respect to the climatological seasonal cycle (reference period 1950–2022).

Soil moisture–temperature coupling

The π diagnostic proposed by Miralles et al.²⁴ was used to assess and quantify the magnitude of soil moisture–temperature coupling. It captures the correlation between soil moisture and temperature and can be used to identify regions where this coupling is particularly strong or weak. The metric is estimated based on near-surface air temperature (T), evaporation (E), potential evaporation (Ep) and surface net radiation (Rn). π is defined as the product of a temperature term (T') and an energy term ($H' - Hp'$):

$$\pi = (H' - Hp')T' \quad (1)$$

where H is the actual sensible heat flux (resulting from the balance between evaporation and surface net radiation), and Hp is the sensible heat that would occur assuming potential evaporation:

$$(H' - Hp') = (Rn - \lambda E)' - (Rn - \lambda Ep)' \quad (2)$$

Where T' , H' and Hp' represent, respectively, the daily anomalies of T , H and Hp expressed in the number of standard deviations relative to their mean, and λE the calculated as a function of T and Rn ³⁸. The derivation of this equation is found in Miralles et al.²⁴ The energy term ($H' - Hp'$) represents, therefore, the short-term potential of soil moisture to affect T through changes in the partitioning of the available radiative energy. When soil moisture is sufficient to meet the atmospheric demand for water, evaporation equals potential evaporation, and the energy term is zero. Under dry conditions, as atmospheric water demand increases and soil moisture gradually decreases, the energy term increases. Ultimately the soil moisture–temperature coupling (π) will be high when positive values of T' concur with high levels of ($H' - Hp'$). This metric was computed on a daily scale and for the contiguous months of March, April and May.

Analogues experiment

We use the analogues approach, which infers the probability distribution of a target field from the atmospheric circulation during a considered time interval³⁹. Flow analogues are days when the atmospheric patterns are similar to those observed during a specific event of interest. They are defined from their root-mean-square differences (RMSD) with respect to the actual Z500 anomaly field at the time of the HW peak event over the following domain: 20W–15E, 25N–50 N. For each day of the HW peak (26–28 April 2023), the search of flow analogues was restricted to a 30-day time window centred on the peak of the event, excluding 2023. Additionally, to address whether the previously accumulated soil moisture deficits over the restricted southern Iberian domain (7.5W–2.5 W, 37.3N–38.6 N) could have contributed to intensifying Tx anomalies over that region at the time of the April HW, we employed the approach proposed by Sousa et al.¹⁸. In this case, we reconstructed Tx anomalies expected from the circulation during the April HW, distinguishing between analogue days preceded by dry and wet conditions. Dry (wet) days are those when the regional mean soil moisture for the previous 15 days is below (above) the 33rd (66th) percentile of the 1950–2022 climatology. For the final selection of analogue days with wet or dry SM preconditions, the 1% (~15 days) of days closest to each of the 3 days of the HW peak were selected. We reconstructed the HW Tx peak 5000 times by randomly choosing one different analogue for each day and for dry and wet preconditions every time to derive flow-conditioned Tx distributions. Following the approach of Sousa et al.¹⁸, we removed the linear trend of the SM time series to conduct the selection of analogues based on wet and dry precedents. This measure was adopted to deal with the impact of long-term trends that could add complexity to the causal relationships between SM and temperature.

We performed several sensitivity analyses to test the robustness of such an approach, mainly to detect any seasonal bias or long-term trend in the selected analogues. A first sensitivity test was based on estimating the annual linear trends of wet and dry analogues mean annual frequency estimated for 21 different sized time windows centred on the peak of the event (i.e., sizes from 20 to 40 days before and after the 26th and 28th, respectively), which proved not to be significant (Supplementary Fig. 5). Additionally, a second sensitivity test was performed to assess if some bias existed in selecting wet and dry analogues preconditions. As the event occurred in a transitional season, wet days tend to be closer to the winter season due to the high dependency of winter precipitation in southern Iberia⁴⁰ whereas dry days increase closer to the summer season⁴¹. In this sense, we tested different daily time windows centred on the peak of the event (20 to 40-day windows) without noticeable differences, indicating a very small bias (<0.1 °C in the southern Iberian Peninsula box) regardless of the size of the time windows (Supplementary Fig. 6), thus increasing the confidence in the results. Finally, we also tested the sensitivity of the analogues technique to the domain size. Thus, we performed the same reconstruction employing 10 different domain sizes (Supplementary Fig. 7) without remarkable differences between them (<0.1 °C in the Iberian Peninsula).

Extreme value analysis

To estimate the probability value of maximum Tx reached over the southern Iberian box during the April HW by considering both wet and dry precedent SM conditions, we employed a non-stationary Generalised Extreme Value (GEV) distribution, a widely used approach to assess the rarity of heat extreme events^{42–44}:

$$G(Tx) = \exp\left(-\left(1 + \xi\left(\frac{Tx - \mu}{s}\right)\right)^{-1/\xi}\right) \quad (3)$$

where $G(Tx)$ represents the cumulative distribution function, μ is the location parameter, σ is the scale parameter, and ξ is the shape parameter. We performed a block maxima approach by selecting the maximum value of each HW peak reconstruction in the analogue procedure. As we reconstructed the HW peak 5000 times for both wet and dry SM preconditions, we obtained 5000 blocks with a maximum reconstructed Tx. Such sets of samples of Tx were then fitted by using the GEV distribution (Supplementary Fig. 8a). In this way, we could infer the probability value of the Tx record in the southern Iberian Peninsula in two different SM precondition contexts (Supplementary Fig. 8b), as well as the ratio between both probabilities (Fig. 4a). Using this same approach, we also predicted the maximum Tx reached for both wet and dry conditions. To this end, given the conditional probability $P(Tx \max | \text{dry})$ of the maximum regional anomaly (13.5 °C) under dry conditions, i.e., for the dry analogues, we inferred the value of $Tx \max | \text{wet}$ in the probability distribution for the wet SM conditions, using the estimated probability $P(Tx \max | \text{dry})$. Then, we calculated the difference between the observed maximum value of Tx and the estimated value of $Tx \max | \text{wet}$ to obtain the amplification value shown in Fig. 4b. This analysis is inspired by the climate change risk-based attribution methodology^{30,31}, but in this case, the probability distributions are compared between groups of dry and wet analogues rather than between a climate with and without anthropogenic forcing.

DATA AVAILABILITY

All data used in this study is publicly accessible online via the following links: AEMET in-situ observations are available through an API request: <https://opendata.aemet.es/centrodedescargas/inicio> SPEI index: <https://monitordesequia.csic.es> ERA5 dataset: <https://cds.climate.copernicus.eu/cdsapp#!/dataset/reanalysis-era5-pressure-levels>. ERA5-Land dataset: <https://cds.climate.copernicus.eu/cdsapp#!/dataset/reanalysis-era5-land>.

CODE AVAILABILITY

All codes used in this study are available upon a reasonable request.

Received: 17 August 2023; Accepted: 7 January 2024;

Published online: 23 January 2024

REFERENCES

- Meehl, G. A. & Tebaldi, C. More intense, more frequent, and longer lasting heat waves in the 21st century. *Science* **305**, 994–997 (2004).
- Fischer, E. M., Sippel, S. & Knutti, R. Increasing probability of record-shattering climate extremes. *Nat. Clim. Change* **11**, 689–695 (2021).
- Valladolid, M. *Spain, Portugal swelter as April Temperature Records Broken*. (Reuters, 2023).
- Philip, S. et al. *Extreme April heat in Spain, Portugal, Morocco & Algeria Almost Impossible without Climate Change*. 11 <http://spiral.imperial.ac.uk/handle/10044/1/103833> <https://doi.org/10.25561/103833> (2023)
- Faranda, D., Pascale, S. & Bulut, B. Persistent anticyclonic conditions and climate change exacerbated the exceptional 2022 European-Mediterranean drought. *Environ. Res. Lett.* **18**, 034030 (2023).
- Dashboard Boletín Hidrológico. <https://miteco.maps.arcgis.com/apps/dashboards/912dfee767264e3884f7aea8eb1e0673> (2023).
- Morocco Ministry of Equipment and Water. Situation journalière des principaux grands barrages—Direction Générale de l'Eau. <https://www.equipement.gov.ma/Pages/accueil.aspx> (Morocco Ministry of Equipment and Water, 2023).
- Coupsures d'eau en Tunisie en raison de la sécheresse. Reuters. <https://www.reuters.com/article/tunisie-eau-idFRKBN2VUORE/> (2023).
- Ministerio de Agricultura, Pesca y Alimentación. El Gobierno aprueba ayudas directas de Estado por más de 636 millones de euros para apoyar a los agricultores y ganaderos frente a la sequía. <https://www.mapa.gob.es/es/prensa/ultimas-noticias/el-gobierno-aprueba-ayudas-directas-de-estado-por-m%C3%A1s-de-636-millones-de-euros-para-apoyar-a-los-agricultores-y-ganaderos-frente-a-la-sequ%C3%ADa/tcm:30-652215> (Ministerio de Agricultura, Pesca y Alimentación, 2023).
- Fischer, E. M., Seneviratne, S. I., Lüthi, D. & Schär, C. Contribution of land-atmosphere coupling to recent European summer heat waves. *Geophys. Res. Lett.* **34** (2007).
- Zscheischler, J. et al. A typology of compound weather and climate events. *Nat Rev Earth Environ* **1**, 333–347 (2020).
- Zhou, S. & Yuan, X. Upwind droughts enhance half of the heatwaves over North China. *Geophys. Res. Lett.* **49** (2022)
- Benson, D. O. & Dirmeyer, P. A. Characterizing the relationship between temperature and soil moisture extremes and their role in the exacerbation of heat waves over the contiguous United States. *J. Clim.* **34**, 2175–2187 (2021).
- Seneviratne, S. I. et al. Investigating soil moisture–climate interactions in a changing climate: a review. *Earth-Sci. Rev.* **99**, 125–161 (2010).
- Miralles, D. et al. Mega-heatwave temperatures due to combined soil desiccation and atmospheric heat accumulation. *Nat. Geosci.* **7**, 345–349 (2014).
- Seo, E. et al. Impact of soil moisture initialization on boreal summer subseasonal forecasts: mid-latitude surface air temperature and heat wave events. *Clim. Dyn.* **52**, 1695–1709 (2019).
- Dirmeyer, P. A., Balsamo, G., Blyth, E. M., Morrison, R. & Cooper, H. M. Land-atmosphere interactions exacerbated the drought and heatwave over northern Europe during summer 2018. *AGU Adv.* **2**, e2020AV000283 (2021).
- Sousa, P. M. et al. Distinct influences of large-scale circulation and regional feedbacks in two exceptional 2019 European heatwaves. *Commun. Earth Environ* **1**, 48 (2020).
- Schumacher, D. L. et al. Amplification of mega-heatwaves through heat torrents fuelled by upwind drought. *Nat. Geosci.* **12**, 712–717 (2019).
- Vautard, R. et al. Summertime European heat and drought waves induced by wintertime Mediterranean rainfall deficit. *Geophys. Res. Lett.* **34** (2007).
- Miralles, D. G., Gentile, P., Seneviratne, S. I. & Teuling, A. J. Land–atmospheric feedbacks during droughts and heatwaves: state of the science and current challenges. *Ann. N.Y. Acad. Sci.* **1436**, 19–35 (2019).
- Barriopedro, D., García-Herrera, R., Ordóñez, C., Miralles, D. G. & Salcedo-Sanz, S. Heat waves: physical understanding and scientific challenges. *Rev. Geophys.* **61** (2023).
- Sánchez-Benítez, A., Barriopedro, D. & García-Herrera, R. Tracking Iberian heatwaves from a new perspective. *Weather Clim. Extremes* **28**, 100238 (2020).
- Miralles, D. G., van den Berg, M. J., Teuling, A. J. & de Jeu, R. A. M. Soil moisture–temperature coupling: A multiscale observational analysis. *Geophys. Res. Lett.* **39** (2012).

- Soares, P. M. M. et al. The future of Iberian droughts: a deeper analysis based on multi-scenario and a multi-model ensemble approach. *Nat. Hazards* **117**, 2001–2028 (2023).
- Andrade, C., Contente, J. & Santos, J. A. Climate change projections of aridity conditions in the Iberian Peninsula. *Water* **13**, 2035 (2021).
- Tabari, H. & Willems, P. Global risk assessment of compound hot-dry events in the context of future climate change and socioeconomic factors. *npj Clim. Atmos. Sci.* **6**, 74 (2023).
- Ruffault, J. et al. Increased likelihood of heat-induced large wildfires in the Mediterranean Basin. *Sci. Rep.* **10**, 13790 (2020).
- Seneviratne, S. I. et al. Land radiative management as contributor to regional-scale climate adaptation and mitigation. *Nat. Geosci.* **11**, 88–96 (2018).
- Stott, P. A., Stone, D. A. & Allen, M. R. Human contribution to the European heatwave of 2003. *Nature* **432**, 610–614 (2004).
- Pall, P. et al. Anthropogenic greenhouse gas contribution to flood risk in England and Wales in autumn 2000. *Nature* **470**, 382–385 (2011).
- Bartusek, S., Kornhuber, K. & Ting, M. 2021 North American heatwave amplified by climate change-driven nonlinear interactions. *Nat. Clim. Change* **12**, 1143–1150 (2022).
- Hauser, M., Orth, R. & Seneviratne, S. I. Investigating soil moisture–climate interactions with prescribed soil moisture experiments: an assessment with the Community Earth System Model (version 1.2). *Geosci. Model Dev.* **10**, 1665–1677 (2017).
- Pizarro Gavilán, M., Hernangómez, D. & Fernández-Avilés, G. *climaemet: Climate AEMET Tools*. <https://doi.org/10.5281/zenodo.5512237> (2021).
- Vicente-Serrano, S. M., Beguería, S. & López-Moreno, J. I. A multiscalar drought index sensitive to global warming: the standardized precipitation evapotranspiration index. *J. Clim.* **23**, 1696–1718 (2010).
- Muñoz-Sabater, J. et al. ERA5-land: a state-of-the-art global reanalysis dataset for land applications. *Earth Syst. Sci. Data* **13**, 4349–4383 (2021).
- Hersbach, H. et al. The ERA5 global reanalysis. *Q. J. R. Meteorol. Soc.* **146**, 1999–2049 (2020).
- Priestley, C. H. B. & Taylor, R. J. On the assessment of surface heat flux and evaporation using large-scale parameters. *Mon. Weather Rev.* **100**, 81–92 (1972).
- Jézéquel, A., Yiou, P. & Radanovics, S. Role of circulation in European heatwaves using flow analogues. *Clim. Dyn.* **50**, 1145–1159 (2018).
- Trigo, R. M. & DaCamara, C. C. Circulation weather types and their influence on the precipitation regime in Portugal. *Int. J. Climatol.* **20**, 1559–1581 (2000).
- Beguería, S., Peña-Angulo, D., Trullenque-Blanco, V. & González-Hidalgo, C. MOPREDAScentury: a long-term monthly precipitation grid for the Spanish mainland. *Earth Syst. Sci. Data* **15**, 2547–2575 (2023).
- Philip, S. Y. et al. Rapid attribution analysis of the extraordinary heat wave on the Pacific coast of the US and Canada in June 2021. *Earth Syst. Dyn.* **13**, 1689–1713 (2022).
- Kew, S. F. et al. The exceptional summer heat wave in southern Europe 2017. *Bull. Amer. Meteor. Soc.* **100**, S49–S53 (2019).
- Van Oldenborgh, G. J. et al. Attributing and projecting heatwaves is hard: we can do better. *Earth's Future* **10**, e2021EF002271 (2022).

ACKNOWLEDGEMENTS

This work frames within the research topics examined by the EXE project funded by the Spanish Ministry of Science and Innovation (PID2020-116860RB-C21). Additionally, this work is also supported by the ATOC project funded by the Barcelona City Council (Ref. 22509371-001). M.L.-C. is supported by a postdoctoral contract from the programme named “Programa de ayudas de apoyo á etapa inicial de formación posdoctoral (2022)” funded by Xunta de Galicia (Government of Galicia, Spain). Reference number: ED481B-2022-055. D.I.-C. is supported by the European Space Agency (ESA) grant no. 4000136272/21/I-EF (CCN. N.1), 4D-MED Hydrology. D.G.M acknowledges support from the European Research Council (HEAT, 101088405). R.M.T was supported by the Portuguese Science Foundation (FCT) through the project AMOTHEC (DRI/India/0098/2020).

AUTHOR CONTRIBUTIONS

M.L.-C. and D.I.-C. jointly wrote the first draft. M.L.-C. performed the data analysis. All co-authors contributed to the discussion and writing/editing of the manuscript.

COMPETING INTERESTS

The authors declare no competing interests.

ADDITIONAL INFORMATION

Supplementary information The online version contains supplementary material available at <https://doi.org/10.1038/s41612-024-00569-6>.

Correspondence and requests for materials should be addressed to Marc Lemus-Canovas.

Reprints and permission information is available at <http://www.nature.com/reprints>

Publisher's note Springer Nature remains neutral with regard to jurisdictional claims in published maps and institutional affiliations.



Open Access This article is licensed under a Creative Commons Attribution 4.0 International License, which permits use, sharing, adaptation, distribution and reproduction in any medium or format, as long as you give appropriate credit to the original author(s) and the source, provide a link to the Creative Commons license, and indicate if changes were made. The images or other third party material in this article are included in the article's Creative Commons license, unless indicated otherwise in a credit line to the material. If material is not included in the article's Creative Commons license and your intended use is not permitted by statutory regulation or exceeds the permitted use, you will need to obtain permission directly from the copyright holder. To view a copy of this license, visit <http://creativecommons.org/licenses/by/4.0/>.

© The Author(s) 2024